Article

DNA−Carbon Nanotube Binding Mode Determines the Efficiency of Carbon Nanotube-Mediated DNA Delivery to Intact Plants

Zahir Ali,◆ Maged F. Serag,◆ Gozde S. Demirer, Bruno Torre, Enzo di Fabrizio, Markita P. Landry, Satoshi Habuchi,* and Magdy Mahfouz*

Cite This: https://doi.org/10.1021/acsanm.1c03482

Read Online

ACCESS | Metrics & More | Article Recommendations | Supporting Information

ABSTRACT: Efficient delivery of DNA, RNA, and genome engineering machinery to plant cells will enable efforts to genetically modify plants for global food security, sustainable energy production, synthetic biology applications, and climate change resilience. For the delivery of functional genetic units into plant cells, nanoparticles, particularly carbon nanotubes (CNTs), have attracted considerable interest. Although some success has been achieved using CNT-based approaches, the efficiency and practicality of the method for genome editing applications remain elusive. This is partly due to insufficient knowledge about the mechanisms of CNT-mediated delivery and expression of CNT-condensed DNA in plants. Here, we characterize the transcription and transformation efficiency of DNA deposited on CNTs coated

with positively charged polymers by applying multiple experimental settings and reporter systems controlling the delivery and expression of DNA in plants. We found that the formation of partially condensed DNA on the CNT surface is a prerequisite for transfection and expression. In addition, we show that DNA irreversibly binds to the CNT and does not detach completely from the CNT surface. These results, together with an *in vitro* transcription assay, suggest that only the partially condensed part of the DNA is accessible to the cellular transcription machinery. Thus, the overall transcription and translation efficiency remains low, in particular for the large DNA units that are required for genome editing applications. Understanding the underlying mechanisms and limitations of CNT-mediated delivery of DNA through the plant cell wall is of considerable importance in guiding efforts to design nanomaterials for efficient transformation, agricultural trait engineering, and synthetic biology applications.

KEYWORDS: *carbon nanotubes, DNA, plant cell, gene delivery, genetic transformation, plants genome engineering, nanobiotechnology*
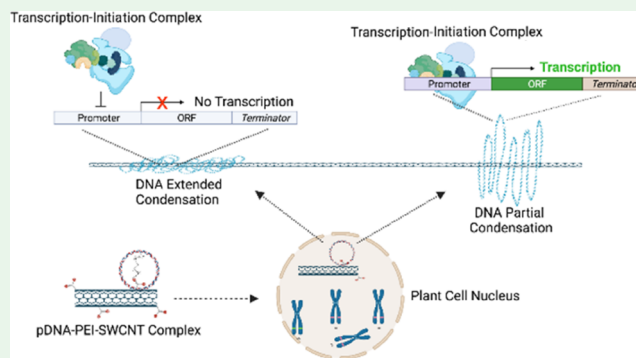
■ INTRODUCTION

Engineering key agronomic traits such as yield and stress tolerance are essential to mitigate the effects of climate change and enhance food security for the growing world population.[1] Moreover, applying the design−build−test−learn cycle of synthetic biology in plants would enable the engineering of plants for traits of value and transform our ability to answer questions and understand plant behavior. Plants can be adopted as low-cost, scalable, and eco-friendly biofactories for various synthetic biology applications, including the production of key biologics and other pharmaceuticals.[2] In addition, genome editing technologies have enabled the production of engineered crop varieties indistinguishable from conventional varieties, thereby simplifying the regulatory landscape.[3] All of these diverse applications require robust methods for the delivery of genetic material, including nucleic acids, functional genetic circuits for synthetic biology, and genome editing reagents, into plant cells.[4] Therefore, establishing an efficient genotype- and species-independent DNA delivery method will transform our

ability to engineer genomes and harness plants for a myriad of applications.

A major barrier for plant genetic engineering is the delivery of genetic materials across the multilayered cell wall into the cell nucleus. The cell wall is porous, with multiple layers of cellulose and pectin polysaccharides with pore sizes of 3.5−9.2 nm.[5,6] Natural mechanisms such as *Agrobacterium tumefaciens* and plant viruses or physical delivery methods such as particle bombardment ("gene gun") and silicon carbide whiskers have been used to deliver genetic cargos into plant cells.[7−9] However, these methods can be labor-intensive and time-consuming, and biotic methods suffer from a limited plant host range whereby abiotic methods have low efficiencies, which complicates and

A

limits their uses in plant engineering.[10] Employing nanotechnology to deliver bioreagents and genetic cargos *via* cell wall pores may address some of these current limitations.

Nanomaterials are defined as materials with at least one dimension that is typically between 1 and 100 nm in size. Their tensile strength, shape, size, surface area, charge, and easy functionalization make these nanomaterials suitable for various technological and biological applications.[11−17] Nanomaterials, including single and multiple walled carbon nanotubes (CNTs), DNA nanostructures, silica nanoparticles, and layered double hydroxide clay nanosheets, have been employed to deliver nucleic acids (DNA and RNA) and other bioreagents into plant cells for diverse applications.[18−22] Similarly, carbon dots were applied to deliver DNA into rice root cells and callus[23] and small RNA molecules to induce RNA interference (RNAi) in mature leaves of model plant *Nicotiana benthamiana* and tomato.[24] Very recently, multiple reports have described the non-biolistic delivery of DNA into plant cells of model and nonmodel plant species without transgene integration using single-walled carbon nanotubes (SWCNTs) for transgene expression in the mature leaf cell cytoplasm or inside the chloroplast and pollen grains.[25−27]

SWCNTs have been widely adopted for the delivery of genetic cargoes. SWCNTs average 1−3 nm in diameter, and their high aspect ratios generate a large surface area to volume ratio for surface chemical functionalization and DNA binding. SWCNTs can be surface-functionalized with different molecules such as arginine or polymers, including polyethyleneimine (PEI) or chitosan, for efficient DNA loading.[26,28−30] In addition to their role in delivery, SWCNTs may also protect DNA from enzymatic degradation in the cellular environment.[31] PEI-functionalized SWCNTs were recently shown to deliver DNA and express a green fluorescent protein (GFP) from a plasmid in intact leaf cells of different plant species.[25,30] In these proof of concept studies, PEI-SWCNT conjugates were used to deliver a 4.2 kb plasmid carrying an enhanced GFP (mutant GFP, mGFP) cassette into the plant cell nucleus, where the expression of the mGFP was detected only in cells treated with PEI-SWCNT-pDNA compared to cells treated with just plasmid DNA and PEI. Similarly, chitosan-SWCNT conjugates were used to deliver a GFP encoding plasmid into chloroplasts, where the release of DNA is favored by the basic pH of chloroplasts (pH 8), resulting in the detection of GFP by fluorescence microscopy in chloroplasts only.[26] Thus, SWCNTs are considered promising carriers for the delivery of DNA plasmids and transient expression of transgenes, including CRISPR-Cas9 genome engineering machinery, into plant cells.[21,25,26,30,32,33] However, most plant genome editing applications require efficient delivery and high expression of multifunctional large DNA constructs into the plant cell, often several times larger than reporter plasmids used for initial proof of concept studies.

In this work, we examined the detailed mechanisms that affect the interaction between large DNA constructs with multifunctional units and SWCNTs coated with the positively charged PEI polymers, the toxicity of the conjugates, the release of DNA from the SWCNT surface, and the expression of functional cassettes of different sizes in plant cells (Scheme 1). Because PEI is a highly charged polymer, we used chitosan, a moderately charged polymer, as a control to validate our results. In addition, DNA can be released from chitosan at the basic pH of chloroplast but not inside the acidic pH of the nucleus. Thus, chitosan can serve as a negative control for the nucleus-based expression of the transformed DNA. Our results demonstrated

Scheme 1. Schematic Illustration Describing the Delivery of Plasmid DNA to Intact Leaf Cells of Plants Using the PEI-Coated SWCNT as a Nanocarrier
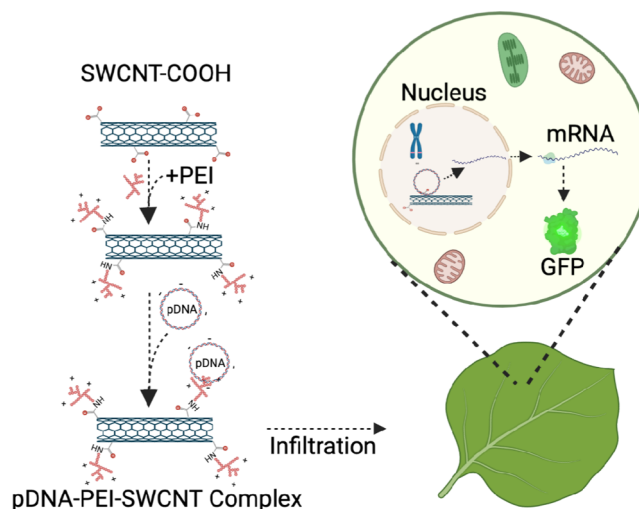
that once condensed on the PEI-CNT, plasmids are not released from the complex, and most of the bounded plasmid part is not accessible for the cellular transcription machinery. Our results highlight the limitations of PEI-CNT-mediated plasmid DNA delivery for practical application in plants and provide clear-cut guidelines for further technological development to establish nanoparticles as carriers for multifunctional DNA plasmids toward genome engineering applications in diverse plant species.

■ RESULTS AND DISCUSSION

Delivery of a Functional DNA Unit into Plant Cells *via* PEI-SWCNTs. To establish that PEI-SWCNTs can be used for DNA plasmid delivery into plant cells, PEI-SWCNT and chitosan-SWCNT conjugates were prepared through amide bond formation between the positively charged polymers PEI (branched, MW 25 000) or chitosan and the carboxylate groups of SWCNTs following the protocols published by Demirer et al.[30] and Kwak et al.[26] Six SWCNT conjugates were made using chitosan (5 mg) and different ratios of PEI (0.1, 20, 30, 40, and 60 mg) with 1 mg of SWCNTs for each (Figure 1a shows atomic force microscopy (AFM) images of PEI_{30} complexed with DNA in 3:1). All of the PEI-SWCNTs were washed multiple times, and the complete removal of free PEI from the solution was confirmed with agarose gel electrophoresis (Figure S1). Next, the 4.2 kb plasmid harboring a GFP cassette was conjugated with the $PEI_{0.1}$-SWCNT, PEI_{30}-SWCNT, PEI_{40}-SWCNT, and PEI_{60}-SWCNT and infiltrated into *N. benthamiana* leaves. Since a previous study demonstrated negative nuclear expression of genes when plasmids were conjugated to chitosan-SWCNTs, we used this complex as a negative control.[26] Confocal microscopy of the PEI-SWCNT-DNA infiltrated leaves confirmed the expression of the mGFP from the 4.2 kb plasmid. A very weak GFP fluorescence was detected in sporadic patches close to the infiltration sites when the leaves were infiltrated with PEI_{30}-SWCNT-DNA but not with chitosan-SWCNT-DNA (Figure S2a). The same conjugates were injected into cotyledonary leaves of cotton (*Gossypium hirsutum*) seedlings. Similar to *N. benthamiana*, confocal microscopy confirmed very low levels of GFP expression in cotton cotyledonary leaves (Figure S2b,c). Next, quantitative reverse transcription polymerase chain reaction (RT-qPCR) was performed to confirm the expression
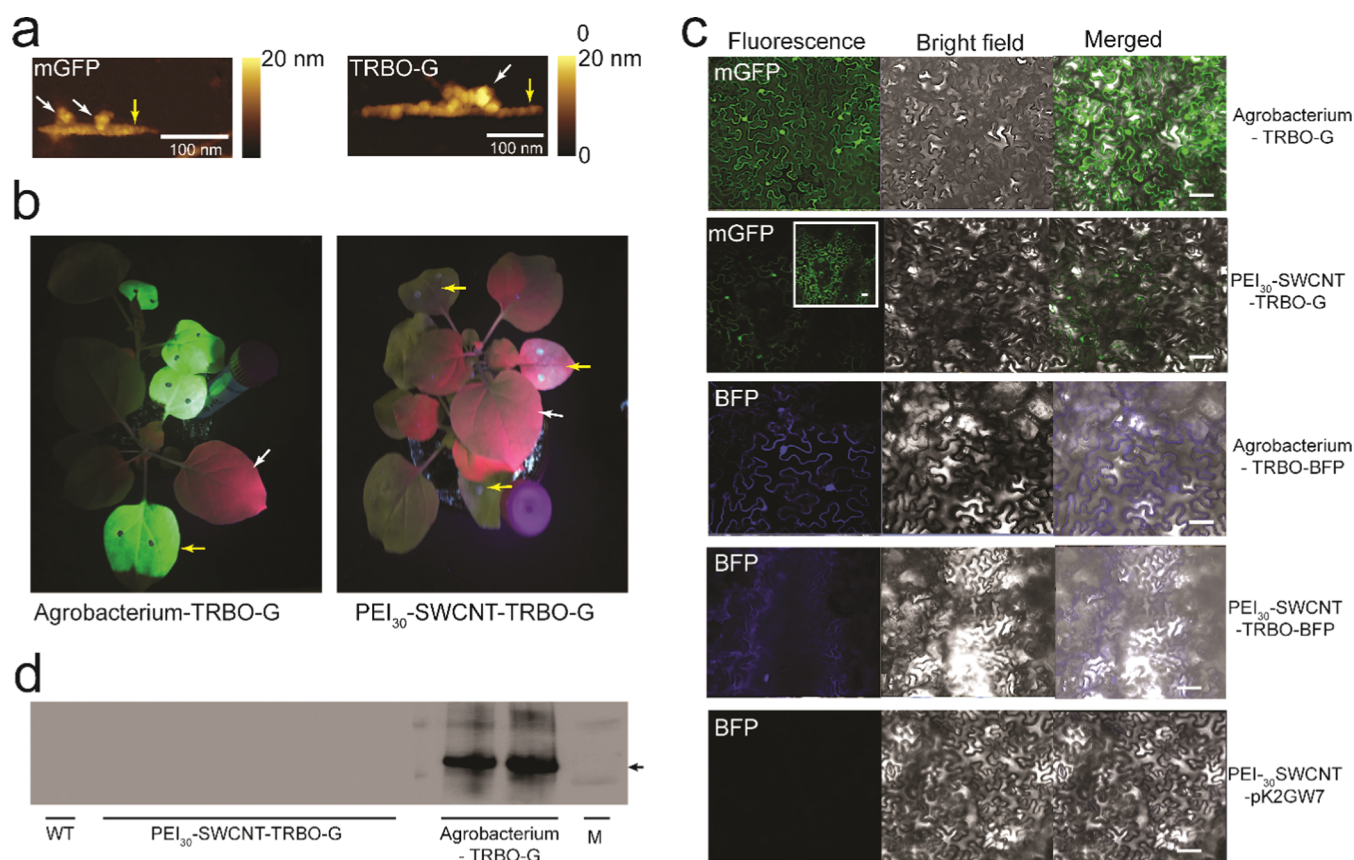
Figure 1. PEI-SWCNT-based delivery of TRBO-G into plant cells. (a) Dry-phase AFM images of the 4.2 kb mGFP plasmid and the 11.3 kb TRBO-G plasmid condensed onto the PEI$_{30}$-SWCNT. The white arrows indicate the condensed plasmid, and the yellow arrows indicate the PEI-SWCNT. (b) TRBO-G delivery into mature plant leaves *via* PEI$_{30}$-SWCNT conjugates. TRBO-G was conjugated with the PEI$_{30}$-SWCNT at a mass ratio of 1:3 (100:300 ng) and infiltrated into two spots of *N. benthamiana* leaves. Pictures were taken under UV light 5 days after infiltration. In the left panel, the yellow arrow indicates a leaf expressing GFP, whereas the white arrows indicate a leaf without a GFP signal under UV light. In the right panel, the yellow arrows indicate the infiltrated leaves with minimal spotted GFP fluorescence, whereas the white arrows indicate a leaf without a GFP signal under UV light. *Agrobacterium* was used as a positive control for the delivery of TRBO-G. The DNA-PEI-SWCNT was infiltrated into two different spots in three individual leaves (yellow arrows) of the same plant. (c) Confocal microscopy images of the leaves infiltrated with the PEI$_{30}$-SWCNT^{+61mV} (the positive number is the measured ζ potential) complexed with TRBO-G or TRBO-BFP plasmids. All images are of 20× magnification, scale bar 100 μm. *Agrobacterium* was used as a positive control for the delivery of TRBO-G and TRBO-BFP. pK2GW7, a plasmid (11 kb) without the GFP cassette, is used as a negative control. The inset demonstrates the image after increasing the gain parameter in microscope software. (d) GFP expression confirmation *via* western blotting. Total extracted proteins were separated by polyacrylamide gel electrophoresis (PAGE) and subjected to western blotting. An anti-GFP antibody was used to detect the expression of the GFP. The arrow indicates the expected GFP in the respective samples. WT denotes wild-type plants, whereas M denotes the protein size marker.

of the GFP. A low level of the GFP expression was detected in *N. benthamiana* samples infiltrated with the PEI$_{30}$-SWCNT-mGFP (4.2 kb) but not with the chitosan-SWCNT-mGFP (4.2 kb) negative control (Figure S3).

The delivery of genome editing reagents and synthetic biology genetic circuits requires the delivery of large constructs, including Cas9, single guide RNA expression cassettes, and repair templates.[34] To test if the PEI$_{30}$-SWCNT enables the delivery of large plasmids in planta, we attempted the delivery of larger plant system compatible plasmids (10−20-kb) than those used in prior studies (4.2 kb). We selected the deconstructed Tobacco mosaic virus (TMV)-GFP TRBO reporter system. The TRBO system is composed of a big, single transcription unit and is a robust fluorescence reporter system that is visually detectable and can confirm both the delivery of a large plasmid into the plant cell and in planta expression of a large functional unit.[35] The TRBO-G plasmid (11.3 kb) was conjugated with PEI-SWCNTs to make a DNA-PEI-SWCNT complex at a 1:3 DNA-to-PEI$_{30}$-SWCNT mass ratio. Atomic force microscopy

(AFM) analysis confirmed that similar to the 4.2 kb plasmid mentioned above, the 11.3 kb plasmid DNA was properly adsorbed onto the PEI-SWCNT surface (Figure 1a and Text S1).

To confirm the delivery and expression of this larger 11.3 kb plasmid DNA with PEI-SWCNTs in planta, the freshly prepared DNA-PEI$_{30}$-SWCNT complex (ratio = 100:300 ng) was infiltrated into *N. benthamiana* leaves. The same 11.3 kb T-DNA construct (the expression cassette of the TMV genome along with the GFP) was transformed into *Agrobacterium* and infiltrated into *N. benthamiana* leaves as infiltration and expression positive control. Translocation of the TMV genome, including the GFP cassette on the T-DNA of the 11.3 kb plasmid *via Agrobacterium*, resulted in the visually detectable expression of the GFP under UV light 3−5 days post-infiltration. Nevertheless, infiltration of the same 11.3 kb plasmid *via* the PEI$_{30}$-SWCNT resulted in a minimal, localized GFP signal around the infiltration site under UV light (Figure 1b). Similarly, in confocal imaging, GFP expression was detected in almost all
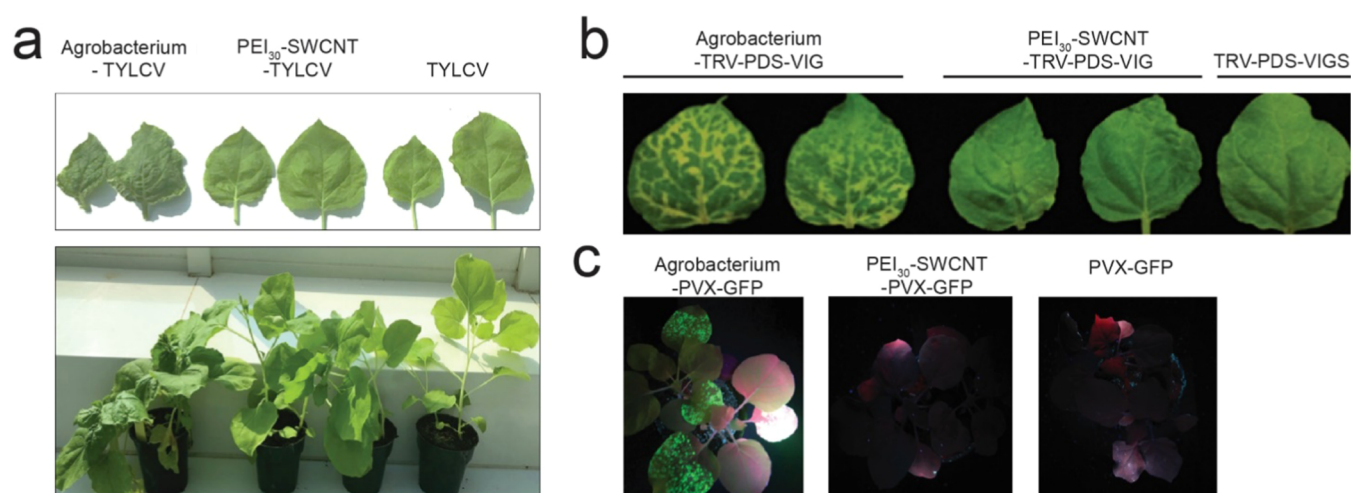
Figure 2. PEI-SWCNT-based delivery of the infectious clones of the DNA and RNA viruses into plants. (a) TYLCV infection in plants. An infectious clone of the TYLCV-harboring plasmid was conjugated with PEI_{30}-SWCNTs and infiltrated into *N. benthamiana* leaves. *Agrobacterium* was used as a positive control to deliver the same binary vector into *N. benthamiana* leaves. The DNA of the TYLCV-harboring plasmid was infiltrated directly into the leaves as a negative control. Top leaf and whole plant pictures were taken 14 days after infiltration. (b) Virus-induced gene silencing (VIGS) in *N. benthamiana* leaves. The phytoene desaturase (PDS) VIGS (modified TRV RNA2, for leaf whitening) and RNA1 clones were conjugated with PEI_{30}-SWCNTs and infiltrated into leaves of 3-week-old *N. benthamiana* plants. VIGS plasmids in *Agrobacterium* were used as a positive control, and VIGS plasmid DNA only was infiltrated directly as a negative control to deliver the same binary vector into *N. benthamiana* leaves. Photos of the top developing leaves were taken 14 days after infiltration. (c) Systemic expression of the GFP in *N. benthamiana* plants. The PVX-GFP clone was conjugated with the PEI_{30}-SWCNT and infiltrated into leaves of 3-week-old *N. benthamiana* plants. The PVX-GFP binary vector in *Agrobacterium* was used as a positive control, and only PVX-GFP plasmid DNA was infiltrated directly as a negative control to deliver the same binary vector into *N. benthamiana* leaves. Photographs were taken under UV light 14 days after infiltration.

of the cells when the construct was translocated *via Agrobacterium*. In contrast, in DNA-PEI_{30}-SWCNT infiltrated leaves, GFP expression was observed only in a few cells, with $0.09 \pm 0.02\%$ (mean $\pm$ standard deviation (SD)) efficiency (relative to *Agrobacterium*-infiltrated leaves, $N = 3$ and 12 for *Agrobacterium* and SWCNT-treated leaves, respectively) (Figure 1c; panels 1 and 2). The efficiency was calculated based on the integrated fluorescence intensity collected from GFP-expressing cells in 10 imaging fields in PEI-SWCNT- and *Agrobacterium*-infiltrated leaves measured 5 days post-infiltration. By increasing the gain parameter in microscope software, the barely detected fluorescence became evident in the PEI_{30}-SWCNT infiltrated cells (inset in Figure 1c). *Agrobacterium* control showed homogeneous GFP fluorescence across the infiltrated leaves because *Agrobacterium* can move in the leaf tissue and spread the TRBO-G. On the other hand, the PEI-SWCNT systems resulted in an inhomogeneous distribution of the GFP fluorescence because the SWCNT bound DNA cassette is localized to the cells in which it has direct contact and, therefore, the expression of the GFP is limited to these cells. Furthermore, while *Agrobacterium* mediated expression results in constitutive GFP expression over 5 days, PEI-CNT based expression is transient and thus peaks and then deminishes within 3 days of infiltration.

To quantify the expression level of GFP, the total RNA was extracted from the respective samples and subjected to RT-qPCR three days post-infiltration. The RT-qPCR results confirmed the very low expression of the GFP in the samples infiltrated with the TRBO-GFP-PEI_{30}-SWCNT complex (Figure S4). To explore these results further, a 10.6 kb nonviral binary vector (pMDC43) harboring a GFP expression cassette was delivered *via* both *Agrobacterium* and PEI_{30}-SWCNTs, and the leaf sections were subjected to confocal imaging 3 days post-infiltration. Confocal microscopy analysis confirmed even less expression of the GFP from a simple binary vector when

delivered *via* the PEI-SWCNT (Figure S5). GFP expression was quantified by RT-qPCR. The RT-qPCR results showed a very low level of GFP expression from the pMDC43-PEI_{30}-SWCNT (10.6 kb, Figure S4), similar to that from the mGFP-PEI_{30}-SWCNT (4.2 kb) plasmid (Figure S3). GFP expression from the TRBO-G-PEI_{30}-SWCNT viral plasmid was slightly high compared with that from PEI_{30}-SWCNT-pMDC43 but remained very low compared with that delivered *via Agrobacterium* (Figure S4).

To further confirm these observations at the molecular level, the total protein was isolated, and the GFP was detected *via* western blotting. Our western blot results did not detect any GFP signal in the DNA-PEI_{30}-SWCNT infiltrated samples (Figure 1d and Text S2). Given no detection with western blot, we sought to validate that the PEI_{30}-SWCNT-based delivery of the viral vector is not an artifact of cell damage, and the detected luminescence is the fluorescent protein signal. To this end, we replaced the GFP in TRBO-G with a blue fluorescent protein (BFP) in the TMV cassette. Infiltration of the TRBO-BFP (11.3 kb *Agrobacterium* system) plasmid *via* the PEI_{30}-SWCNT also resulted in low expression in the cells with $0.05 \pm 0.06\%$ efficiency of the BFP relative to the *Agrobacterium* system as measured by confocal microscopy (Figure 1c; panels 3 and 4). As a control, no GFP or BFP signal was detected in the leaves infiltrated with plasmid pK2GW7 (without the fluorescent protein gene) conjugated with the PEI_{30}-SWCNT (Figure 1c; panel 5). Based on the above assays, our results suggest a very low expression of large functional DNA cassettes (10.6 and 11.3 kb plasmids) when delivered with the PEI-SWCNT system. Taken together, the expression of reporter genes from plasmids (both 4.2 and 12 kb) complexed to the PEI_{30}-SWCNT is weak when compared with *Agrobacterium*.

PEI is the determining factor in DNA binding to SWCNTs.[30] To confirm that the ratio of PEI to SWCNTs used in the
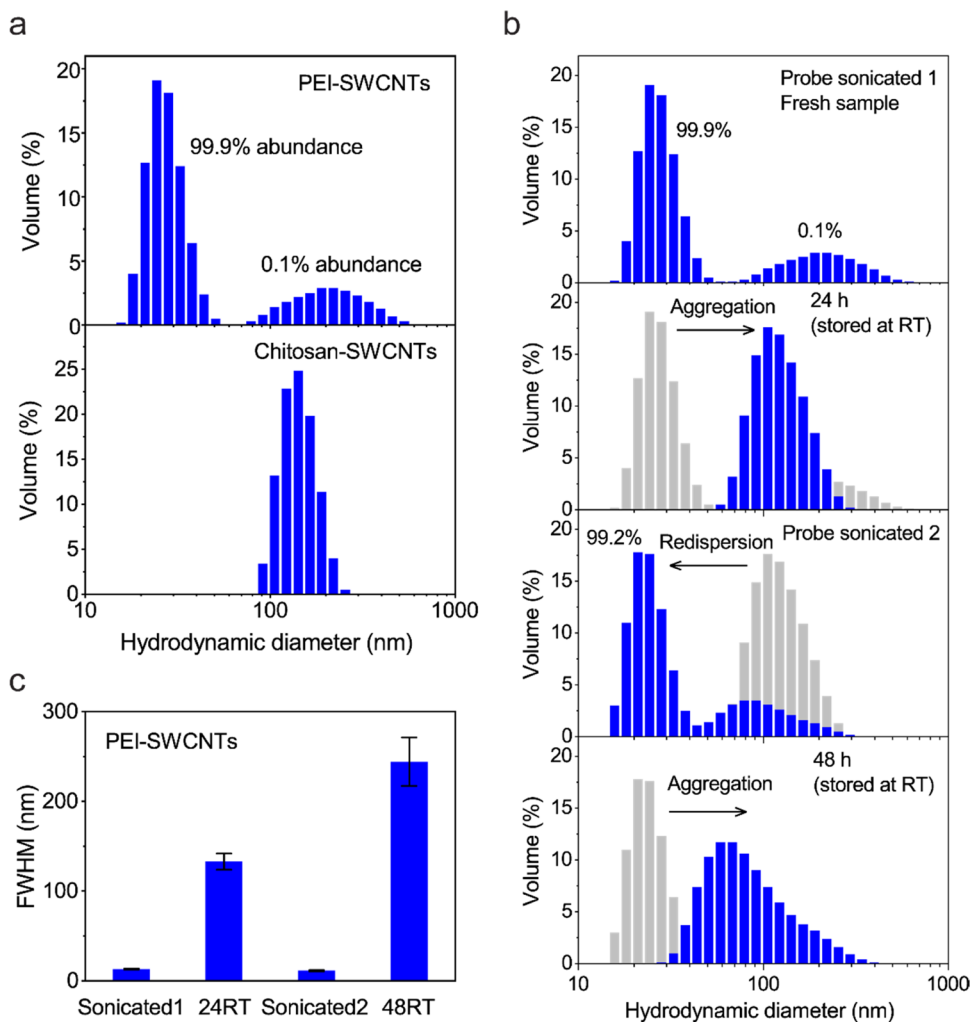
Figure 3. Hydrodynamic diameter and aggregation of polymer-coated carbon nanotubes. (a) Distribution of the hydrodynamic diameter of PEI-SWCNTs (30:1 mass ratio) and chitosan-SWCNTs. Measurements were taken immediately after the synthesis and probe-tip sonication. The polydispersity indices of PEI-SWCNTs and chitosan-SWCNTs are 0.3 and 0.2, respectively. (b) Distribution of the hydrodynamic diameter of PEI$_{30}$-SWCNTs at different incubation periods (24 and 48 h). Following each incubation period, each composite was probe sonicated for 5 min. (c) Full width at half-maximum (FWHM) of the predominant hydrodynamic diameter distribution (>99% volume) of PEI-coated SWCNTs shown in (b). Freshly synthesized and sonicated PEI$_{30}$-SWCNTs showed a small FWHM.

synthesis of the PEI-SWCNT conjugate and delivery of the plasmid is not responsible for the low expression of the GFP signal, we synthesized DNA-PEI-SWCNT complexes with different ratios of the PEI-SWCNT (PEI$_{30}$-SWCNTs, PEI$_{40}$-SWCNT, and PEI$_{60}$-SWCNT), each loaded with 100 ng of TRBO-G plasmid DNA and 300 ng of individual PEI-SWCNT, and infiltrated 100 μL of the solution into *N. benthamiana* leaves. We observed a low level of expression from the PEI-SWCNT at all concentrations of PEI and leaf tissue damage with morphological changes with the two highest PEI concentrations (PEI$_{40}$-SWCNT and PEI$_{60}$-SWCNT), hindering proper imaging of the respective cells (Figure S6). Our results highlight the PEI-induced physical damage of tissues when used at high concentrations. We note that we always took the bright field images as a guide to image only healthy leaf tissues so as to discern whether the fluorescence signal we detected was due to tissue damage or a genuine GFP signal.

Delivery of Plant Virus Reporter Systems *via* PEI-SWCNTs. The extremely low in planta expression (<0.1% efficiency compared to *Agrobacterium*) of the functional DNA unit delivered *via* PEI$_{30}$-SWCNTs prompted us to investigate

the mechanism of the PEI-SWCNT-based DNA delivery and expression in plant cells in more detail. In nature, insect vectors are the main source of virus transmission in plants.[36] Insect vectors generally transmit very few copies of the virus particles into plant cells. However, inside the plant cell, the robust replication system of the viruses hijacks the plant cellular machinery to rapidly produce virus particles.[37,38] Thus, a few copies delivered into the cell nucleus result in significant reporter readout independent of the concentration (or number) of the delivered DNA. We reasoned that the intracellular release of an infectious virus genome from PEI$_{30}$-SWCNTs at an efficiency lower than the observed <0.1% efficiency (Figure 1c) would be sufficient to initiate virus replication inside the plant cell. Different plant viruses (reporter clones) were selected to distinguish between the two possible mechanisms for the low level in planta expression of the functional DNA unit (*i.e.*, the release of a low number of DNA molecules or low expression of the long functional units from DNA conjugated PEI$_{30}$-SWCNTs). Tomato Yellow Leaf Curl Virus (TYLCV) is a DNA virus, and the replication and systemic movement of TYLCV in plants result in leaf thickening, cup-shaped curling,

and dwarfing.[39] The binary plasmid (11 kb) harboring the infectious TYLCV clone was conjugated at 1:3 ratio with PEI_{30}-SWCNTs and infiltrated into *N. benthamiana* leaves. The same clone DNA was directly infiltrated as a negative control and also transformed into *Agrobacterium* and infiltrated into *N. benthamiana* leaves as a positive control. Seven days following infiltration, compared to the typical TYLCV symptoms in plants infiltrated with *Agrobacterium* carrying a TYLCV infectious clone, plants infiltrated with the TYLCV plasmid DNA conjugated PEI_{30}-SWCNTs developed no symptoms (Figure 2a). To confirm these observations at the molecular level, the total DNA was isolated, and the presence of the TYLCV genome was detected *via* a rolling circle amplification (RCA) assay. The RCA assay did not amplify the TYLCV genome in the DNA-PEI_{30}-SWCNT infiltrated samples (Figure S7), confirming no release of the viral DNA or unavailability of viral DNA to the cellular replication machinery.

The plasmid DNA delivered *via* PEI-SWCNTs was reported to be expressed transiently without integration into the genome.[25,30] Therefore, it is possible that the DNA vector does not detach from PEI-SWCNTs and that the vector's functional units are expressed from the DNA while it is conjugated with PEI-SWCNTs but not from free DNA molecules. To consider this possibility, we used two clones of RNA viruses, Tobacco rattle virus (TRV) and Potato virus X (PVX). Once expressed inside the plant cell from a DNA molecule, the RNA genome of these viruses replicates independently. The use of RNA viruses can provide an excellent system to explore the possibility of low expression of large functional units from the DNA-PEI-SWCNT. Modified TRVs can provoke virus-induced gene silencing (VIGS) of phytoene desaturase (PDS) gene transcripts and lead to systemic silencing of PDS transcripts resulting in whitening of the leaves of *N. benthamiana*.[40] To confirm that the extremely low initial transcription of the RNA genome can lead to the establishment of VIGS in *N. benthamiana*, TRV-PDS VIGS clones were conjugated with the PEI_{30}-SWCNT. The conjugates were infiltrated into *N. benthamiana* leaves. As a positive control, the same clones were transformed into *Agrobacterium* and only VIGS plasmid DNA as a negative control were infiltrated into *N. benthamiana* leaves. Infiltration of the TRV-PDS-PEI_{30}-SWCNTs did not initiate the PDS transcript-based whitening in *N. benthamiana* leaves compared to the observed whitening of the leaves in plants infiltrated with *Agrobacterium* containing the TRV-PDS VIGS system (Figure 2b). To reconfirm our experimental observations, another RNA virus PVX-GFP system was selected, whereupon successful infection, PVX resulted in the systemic spread of the GFP to the whole plant.[41] Similar to no infection from TYLCV and TRV, infiltration of the PVX-GFP-PEI_{30}-SWCNT did not result in any expression and systemic movement of the GFP in *N. benthamiana* plants (Figure 2c).

Taken together, these observations demonstrated that when bound to PEI_{30}-SWCNTs, some or all functional units of the plasmid DNA are not accessible to the cellular machinery as a single unit for replication and expression. Similarly, the large functional unit residing on the plasmid DNA is not available for transcription to initiate the RNA-based genomic replication of TRV and PVX viruses. These results indicate that DNA condensation on PEI-SWCNTs does not allow the release of DNA, and the bound DNA is not available as a single unit for replication and transcription machinery. Since these findings may imply a fundamental limitation of the PEI-SWCNT-based

in planta expression of large plasmids, we decided to conduct a deep investigation of the mechanisms of binding, release, and expression of DNA.

Aggregation of PEI-SWCNT Composites. A major drawback associated with carbon nanotubes is their aggregation in aqueous solutions. Aggregation of carbon nanotubes can increase toxicity[42] and decrease transformation efficiency because of precipitation.[25] Thus, we investigated the surface charge and the size of the PEI-SWCNT composites *via* ζ potential measurements and atomic force microscopy prior to addressing the binding mode of DNA to the PEI-SWCNTs.

ζ potential measurements of all PEI-SWCNT composites and chitosan-SWCNT composites showed values of 50−77 and 35−38 mV, respectively. Although the ζ potential of PEI-SWCNTs was more positive than that of chitosan-SWCNTs, the chitosan-SWCNTs showed better stability and remained well dispersed in solution when stored for several days at room temperature (hydrodynamic diameter of chitosan-SWCNTs (d) = 150 nm, Figure 3a and Text S3). Conversely, all PEI-SWCNTs were prone to fast aggregation where the hydrodynamic diameter measurements showed an increase of tenfold (from 15 to 150 nm) when stored at room temperature for 24 h (Figure 3b). However, these aggregates were shown to transiently disperse when the solution was briefly probe-tip sonicated for 5 min (Figure 3b,c). See Text S4 for a detailed discussion on the physical differences between the PEI-SWCNTs and chitosan-SWCNTs, their role in the organization of the ion layers around the composites, and how these differences affect the dynamic light scattering data and DNA loading.

Consistent with earlier investigations of both SWCNT-polymer composites, AFM imaging showed no difference in the height of PEI_{30}-SWCNTs and chitosan-SWCNTs (AFM height h = 5 nm).[25,26] The identical AFM height values are in contrast to the different hydrodynamic diameter values of 15 and 150 nm of the PEI-SWCNT and chitosan-SWCNT, respectively. This indicates a different thickness of the ion layers surrounding the polymer-coated SWCNT (Text S4). While both PEI_{30}-SWCNTs and chitosan-SWCNTs showed a high positive ζ potential, the AFM images revealed that only PEI_{30}-SWCNTs exhibited aggregations along their sidewalls (C.F. carboxylated SWCNT (ζ = −70 mV), Figure S8). We found that PEI-SWCNT preparations with inefficient sonication and with a hydrodynamic diameter greater than ∼15 nm (*i.e.*, contains aggregates; Figure 3b (panels 2 and 4) and ST3c,d) precipitated over time. We also found that an efficient probe-tip sonication rather than bath sonication is essential to generate a colloidal dispersion of PEI-SWCNTs.

The aggregation behavior of the PEI-SWCNT could be explained by ion condensation theory (see Text S4).[43] According to the theory, aggregation is promoted due to the development of a layer of strongly held counterions on highly charged one-dimensional rod-like PEI-SWCNT polyelectrolytes in solution. When the surface charge of the PEI-SWCNT is sufficiently high, a strongly attractive, long-range Coulomb force develops between highly charged rod-like polyelectrolyte molecules bearing similar charges.[43] This attractive force explains the like-charge aggregation of the highly charged PEI-SWCNT (Figure S8). It is likely that the aggregation tendency of the PEI-SWCNT is one of the major reasons for non-reproducible results. In addition, this condensed counterion layer has an extremely small thickness when compared with the diffuse ion layer of moderately charged polyelectrolytes such as the chitosan-SWCNT^{+38mV} (Text S4 and Figure 3a). The
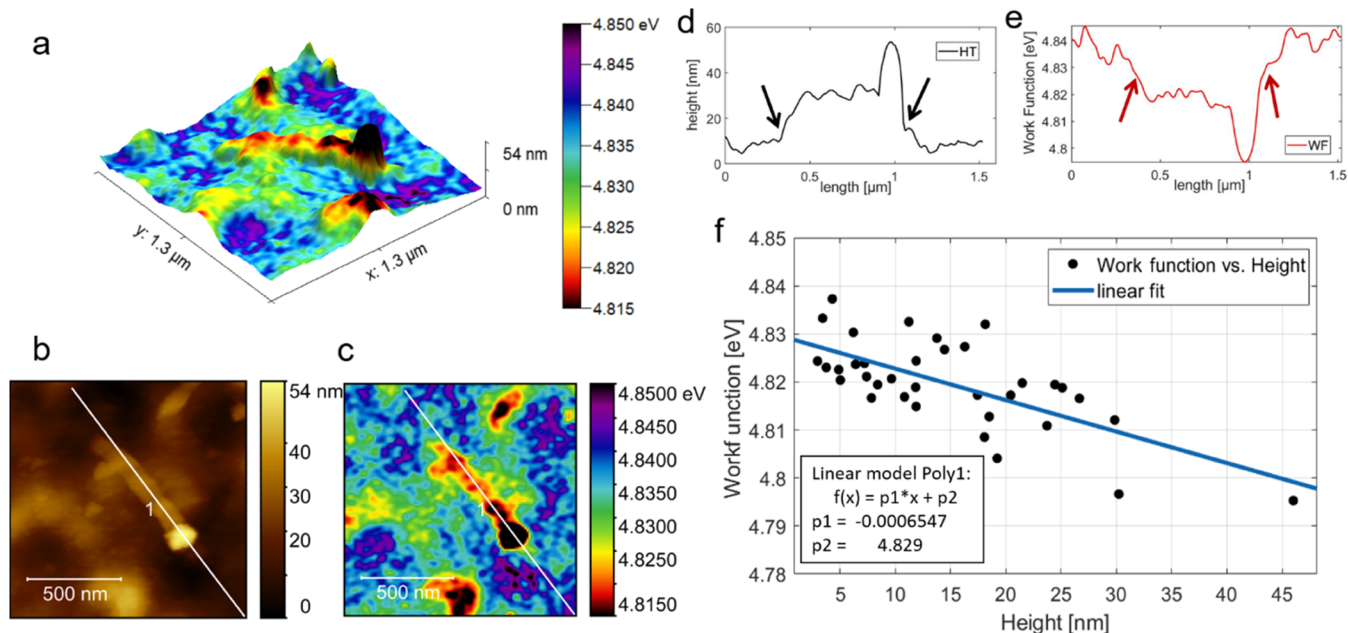
Figure 4. Correlation between PEI thickness and work function in PEI-SWCNTs. (a) 3D rendering of a representative PEI$_{30}$-SWCNT: work function, in color scale, shows the correlation between coating thickness and electrical properties. (b) Topography, (c) work function, (d) height profile, and (e) work-function profile quantitatively showing the (anti-)correlation of the dry-phase AFM topographic image between the thickness and surface potential. Black (d) and red (e) arrows are placed in correspondence of the two ends of the PEI$_{30}$-SWCNT. (f) Work function *vs* height correlation statistics extracted from the 10 PEI$_{30}$-SWCNT in different sample locations. A simple first-order polynomial regression (blue line) shows and quantifies the dependence coefficient to -0.66 meV nm^{-1}, where the minus sign expresses the anticorrelation between the two parameters.

relatively smaller hydrodynamic diameter of the PEI-SWCNT could facilitate the passage of the PEI-SWCNT through cell wall pores, whereas the larger hydrodynamic diameter of chitosan-SWCNTs could hinder the passage of chitosan-SWCNTs.

Mixing the PEI$_{30}$-SWCNTs with the 11.3 kb TRBO-G plasmid DNA also caused aggregations. AFM and hydrodynamic diameter (d) measurements showed a progressive aggregation with a subsequent increase of d upon the increasing concentration of plasmid DNA. The PEI-SWCNT/DNA ratio of 3:1 showed a minimal increase of d after adding DNA, whereas ratios as low as 1:1 showed significant aggregation with an increase of d ($d = 300$ nm, Figure S9a,b), and thus those preparations could not be infiltrated into plant tissues because of precipitation out of the solution (Figure S9c).

Binding Modes of DNA on PEI-SWCNT Composites. To investigate the binding interactions of DNA and the positively charged PEI-SWCNT composites, we first studied the effect of PEI on the surface charge of the PEI-SWCNT composites. The AFM height and ζ potential of PEI-SWCNTs increased from $h = 3.5 \pm 1.2$ nm, $\zeta = +52$ mV to $h = 4.4 \pm 2$ nm, $\zeta = +61$ mV when the reaction time of activated PEI and SWCNTs (20:1 w/w) increased from 12 to 18 h (denoted PEI$_{20}$-SWCNT^{+52mV} and PEI$_{20}$-SWCNT^{+61mV}, respectively (statistical data shown in Figure S10)). These values are consistent with the ζ potentials reported previously.[30] Note that throughout the manuscript, we use the ζ potential value as a superscript, whereas we use the ratio of the PEI/SWCNT as a subscript. Similarly, increasing the mass ratio of the PEI/SWCNT to 40:1 w/w increased both the AFM height and ζ potential to $h = 5 \pm 1.8$ nm, $\zeta = +77$ mV (denoted PEI$_{40}$-SWCNT^{+77mV}, statistical data shown in Figure S10a−c). By contrast, decreasing the mass ratio to 1:10 resulted in a segmented coating of PEI (Figure S11) with a concomitant decrease in the measured ζ potential to $\zeta = +30$ mV (PEI$_{0.1}$-SWCNT^{+30mV}).

Using Kelvin probe force microscopy (KPFM), we observed local variation in the surface potential of the PEI-coated CNTs concomitant with local variation in the thickness of the PEI coating layer in the range of 3−50 nm (75% of the height values lie within the range of 3−20 nm). In this experiment, we used the PEI$_{30}$-SWCNT^{+61mV} because the infiltration of this conjugate resulted in the best GFP expression in terms of the brightness of the GFP fluorescence signal and lower toxicity (Figure 1a,c). Figure 4 shows the correlation between the PEI height and local work function of the sample in a representative area of the sample, visible in both in the three-dimensional (3D) rendering of the work function on the topography (Figures 4a and S10d−f) and in the line profiles of the work function and topography (Figure 4b−e). The KPFM imaging experiment on 35 PEI-SWCNTs demonstrated a negative correlation between the PEI height (in the range of 3−47 nm) and the work function (Figure 4f), which confirms the anticorrelation shown in the line profiles (Figure 4d,e). This negative correlation, *i.e.*, the decrease in the work function with the thickness, represents the tendency to accumulate more positive charge[44,45] in the thicker part of PEI coating. We also found potential (charge) fluctuations along the same PEI$_{30}$-SWCNT (Figure 4e). Because of this local variation in the surface potential, we posited that DNA could show various binding modes and strengths to the surface of the PEI$_{30}$-SWCNT functionalized with different thicknesses of the PEI polymer.

To investigate whether the plasmid DNAs have different binding modes to PEI-SWCNTs, we recorded AFM tapping mode images of composites with different PEI surface modifications and ζ potentials. DNA binds to the chitosan-CNT^{+38mV} in an extended conformation with no extrusions along the surface of the nanotubes (Figure 5a−c), which is consistent with previous investigations.[26] Similarly, DNA binds to PEI-coated SWCNTs at 20:1 and 30:1 mass ratios with a ζ
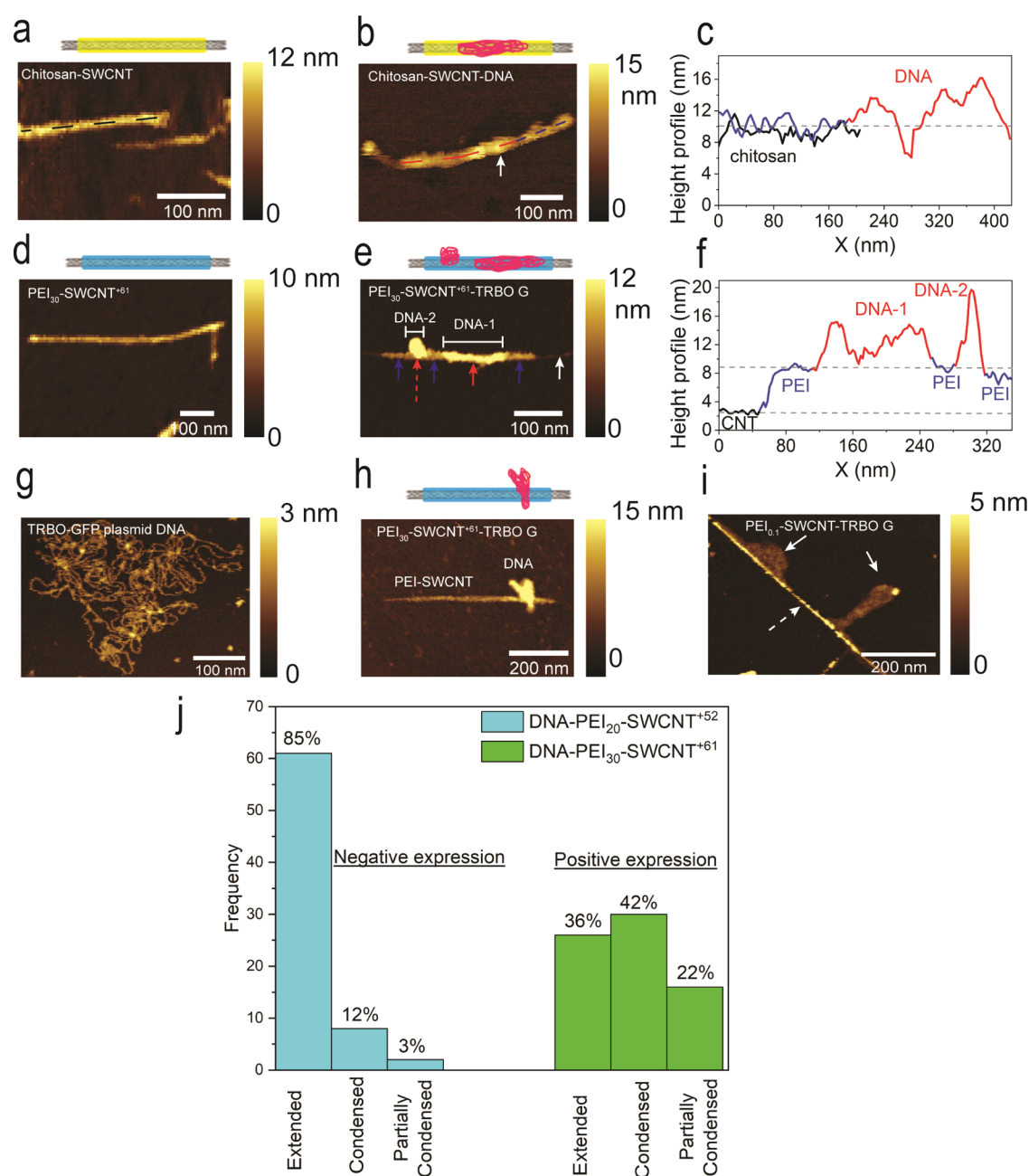
Figure 5. Different binding modes of DNA to PEI-SWCNTs. (a) Dry-phase AFM topographic image of chitosan-SWCNTs dispersed in water. The height profile along the dashed line is shown in (c). (b) Dry-phase AFM topographic image of a chitosan-SWCNT-DNA complex. The arrow indicates DNA extended along the surface of the chitosan-SWCNT. (c) Height profile of the chitosan-SWCNT and the DNA-chitosan-SWCNT complex along the dashed lines (color-coded) shown in (a) and (b). (d) Dry-phase AFM topographic image of a single PEI_{30}-$SWCNT^{+61mV}$. (e) Dry-phase AFM topographic image of a PEI_{30}-$SWCNT^{+61mV}$-TRBO-G DNA complex. The white arrow indicates the SWCNT. The blue arrows indicate coating layers of PEI. The solid red arrows indicate DNA extended along the surface of the PEI_{30}-SWCNT. The dashed red arrow indicates DNA condensed on the surface of the PEI_{30}-SWCNT. (f) Height profile of the PEI_{30}-$SWCNT^{+61mV}$-TRBO-G DNA complex between the arrowheads is shown in (e). (g) Liquid-phase AFM topographic image of the TRBO-G GFP plasmid. (h) Dry-phase AFM topographic image of a partially condensed PEI_{30}-$SWCNT^{+61mV}$-TRBO-G DNA complex. Note that (e) (extended and condensed modes of binding) and (h) (partially condensed mode of binding) were obtained from the same PEI_{30}-$SWCNT^{+61mV}$ sample. (i) Dry-phase AFM topographic image of the TRBO-G GFP plasmid attached to the $PEI_{0.1}$-$SWCNT^{+30mV}$. The solid arrows indicate DNA, whereas the dashed arrow indicates a single PEI-SWCNT, which shows a segmented coating with PEI. Schematics are included for the interpretation of AFM data. (j) Frequency distribution of different modes of binding of TRBO-DNA to the PEI_{20}-$SWCNT^{+52mV}$ and PEI_{20}-$SWCNT^{+61mV}$. To obtain the frequency distribution shown in (e), we imaged the DNA-PEI_{20}-SWCNT and DNA-PEI_{30}-SWCNT, which showed negative and positive expression results, respectively. We obtained approximately 100 images of each preparation and identified 70 tubes in each sample. We then determined the number of extended, condensed, and partially condensed modes of DNA in each subset of images. See Figure S16 for additional AFM images of the partially extended mode of DNA binding with lobes of DNA extruding from the PEI_{30}-SWCNT.

potential of +52 mV and with ζ potential ranging between +50 and +60 mV, respectively, in an extended conformation manner

(Figures S12a,b and S13a and Text S5). This type of condensation did not show the expression in the plant cells

(Table S1, row 6, Figure S12c, and Appendix S1). By contrast, PEI-SWCNTs with larger ζ potentials ($\zeta > +60$ mV) showed different binding modes of DNA. We found that DNA binds to the PEI$_{20}$-SWCNT^{+61mV}, PEI$_{30}$-SWCNT^{+61mV}, and PEI$_{40}$-SWCNT^{+77mV} in a condensed, partially condensed, and extended manner, respectively (Figures 5d−h and S13b−d and Appendix S2). Importantly, these binding modes coexist on these PEI-SWCNTs (Figure 5e,h). Unlike the extended conformation of DNA binding where DNA is partially exposed to the buffer solution with no extrusions (*e.g.*, Figures 5e (DNA-1), S12a, and S13a), condensed and partially condensed DNA conformations showed extrusions (Figures 5e (DNA-2),5h and S14). We observed GFP expression when the PEI$_{30}$-SWCNT^{+61mV} and PEI$_{40}$-SWCNT^{+77mV} were complexed with plasmid DNA and infiltrated into plant leaves (Figure 1b,c). When the PEI/SWCNT mass ratio was decreased to 0.1:1 (PEI$_{0.1}$-SWCNT^{+30mV}, Figure 5i), the DNA extrusions increased in size concomitant with the loose binding of DNA to PEI-SWCNTs where the infiltrated leaves did not show any sign of GFP expression (Figure S15). Frequency histograms of the DNA binding modes to the PEI-SWCNT (Figure 5j) statistically demonstrated that DNA on the PEI$_{20}$-SWCNT^{+52mV} (that displayed negative transformation) predominantly displayed the extended binding mode (85%), whereas a minor fraction (15%) of DNA was found to bind to the PEI$_{20}$-SWCNT in either condensed or partially condensed modes. The relative contribution of the condensed and partially condensed DNA in the DNA-PEI$_{20}$-SWCNT is close to the error of 13% that an artifact is identified as a condensed DNA (Text S1). In contrast, the majority of DNA bound to the PEI$_{30}$-SWCNT^{+61mV} (that displayed positive transformation) in either condensed (42%) or partially condensed (22%) modes. We note that *in situ* characterization of the binding modes of DNA to the PEI-SWCNT using liquid-phase AFM did not work because of the interaction between the injected plasmid DNA and the AFM probe during the incubation period, which hampered the AFM imaging experiment.

Our AFM measurements and transformation results (Figures 1, 4, 5, and S12−S16 and Appendices S1 and S2) suggest a strong correlation between the ζ potential values, mode of plasmid DNA binding to the surface of PEI-SWCNTs, and the efficiency and reproducibility of transformation. Because the binding of plasmid DNA neutralized the local charge of PEI-SWCNTs, we were not able to assign a specific mode of binding to a specific range of local surface potentials (Text S6). Nevertheless, the partially condensed and condensed DNA were observed predominantly in the PEI-SWCNT composites of high ζ potentials (PEI$_{30}$-SWCNT) with a relative abundance of 64% (C.F. 15% in PEI$_{20}$-SWCNT composites of lower ζ potential); meanwhile, a nonuniform height and surface potential distribution exist along the surface of individual PEI-SWCNTs. Thus, we posit that the condensed and partially condensed DNA binding modes are linked to the zones of PEI-SWCNTs with higher positive surface charges, whereas the extended DNA binding mode is linked to zones of PEI-SWCNTs with moderate positive surface charges. Although the partially condensed DNA is much smaller in size than the free plasmid DNA (Figure 5g), our observations indicate that the partially condensed DNA shows extrusions that allow for the expression of DNA in the plant cell (Figures 5h, S2, S6, and S14). The negative expression results observed for the PEI$_{0.1}$-SWCNT^{+30mV} could be due to the inability of the larger DNA-PEI-SWCNT complex (*i.e.*, ~200 nm physical size of the bound DNA, Figure 5i) to get through

the plant cell wall pores. Our findings also indicate that the DNA sequence has little effect on the binding modes because the binding is purely Coulombic between the negative charges of the phosphate backbone of DNA and the positively charged PEI molecules.

Investigation of the Effect of Buffer Conditions on the Expression of the GFP. Following electrophysical characterization, which suggested that the SWCNT surface charge plays an important role in the binding mode of DNA and its resulting accessibility for expression and transformation, we investigated whether the physical factors and charges in the solution could play a role in enhancing gene expression. We investigated the inherent variability in the DNA-PEI-SWCNT complex infiltrated into *N. benthamiana* leaves. To that end, multiple preparations of the PEI$_{30}$-SWCNT were conjugated with the TRBO-G plasmid DNA and infiltrated into *N. benthamiana* plant leaves. The different PEI-SWCNT preparations showed diverse expression results, with 2 of the 19 conditions tested yielding consistent expression, as summarized in Table S1. Next, to confirm whether the infiltration buffer composition limited plasmid delivery and transgene expression in plant cells, the PEI$_{30}$-SWCNT^{+61mV} was mixed with the DNA plasmid in water as a solvent (ζ = +61 mV, Figure S17), half-strength 2-morpholinoethanesulfonic acid (MES) buffer (MES 12.5 mM and MgCl$_2$ 7.5 mM, pH 6, ζ = +51 mV, Figure S17), and full-strength MES buffer (MES 25 mM and MgCl$_2$ 15 mM, pH 6, ζ = +41 mV, Figure S17) and infiltrated into *N. benthamiana* leaves. We note that these ζ potential values were measured at different salt concentrations without DNA. In our experiments, we added the buffer and DNA simultaneously to the water solution of PEI-SWCNTs (ζ = +61 mV). The DNA-PEI$_{30}$-SWCNT complex infiltrated in the half-strength MES buffer consistently exhibited higher GFP expression than the full-strength MES buffer and water only used as infiltration buffer (Figure S18). Almost all leaf slices showed the GFP signal when the half-strength MES buffer was used, whereas only a limited area exhibited the GFP signal when full-strength MES buffer was used (Figure S18). Next, the total RNA was isolated and the GFP expression was detected *via* RT-qPCR three days post-infiltration. RT-qPCR results showed that the expression of the GFP in the half-strength MES buffer was enhanced by a factor of 2 and 4 compared with those in full-strength MES buffer and water, respectively (Figure S4).

Concomitant with our previous results that the partially condensed DNA remains exposed and thus available to the buffer solution (Figure S14), the divalent ions (Mg^{2+}) in the buffer act as counterions that can attract uncondensed negatively charged domains of the bound DNA leading to aggregation. A 2-fold increase of the DNA resulted in the precipitation of the DNA-PEI$_{30}$-SWCNT out of the solution (Figure S9c), whereas reducing the Mg^{2+} concentration in the half-strength MES buffer decreased the aggregation and enhanced the expression efficiency (see Figure S18).

Investigation of the Potential Release of DNA from PEI-SWCNT Composites. To investigate whether the bound DNA can be released from the PEI$_{30}$-SWCNT and whether one binding mode favors DNA release, we condensed an equal amount of plasmid DNA on the freshly prepared PEI$_{30}$-SWCNT^{+61mV}. The complexes were subjected to ethidium bromide (EtBr)-based detection in agarose gel electrophoresis. The absence of the respective DNA fragment on the gel confirmed the efficient condensation of DNA onto the PEI-SWCNT compared to the bare plasmid control (Figure S19a). As an alternative to the gel assay, the PEI$_{30}$-SWCNT^{+61mV}-DNA
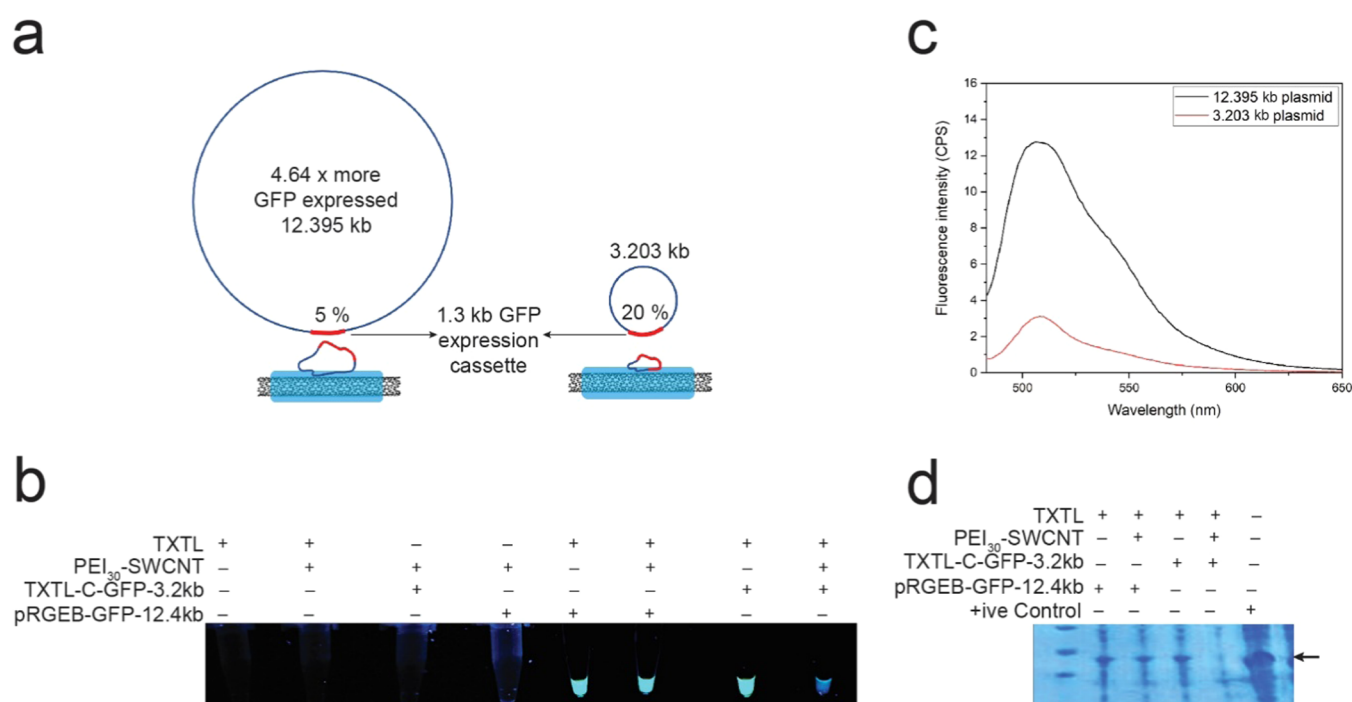
Figure 6. Determination of the availability of DNA functional units for expression. (a) GFP expression cassette (pQ70-deGFP-terminator, 1.3 kb fragment) was cloned to make a small (3.2 kb) plasmid and a large (12.4 kb) plasmid. The GFP cassette constituted 5% of the large plasmid and 20% of the small plasmid. (b) *In vitro* transcription and translation of the GFP cassette. The constructed clones were conjugated with the PEI_{30}-$SWCNT^{+61mV}$ and subjected to a TXTL *in vitro* transcription assay and translation along with the respective controls. Pictures were taken under a UV light after 16 h of incubation. Unconjugated plasmids (3.2 and 12.4 kb) were used as a control (columns 5 and 7). (c) Fluorescence spectra of the GFP expressed from the GFP cassette cloned into the 3.2 kb (red) and 12.4 kb (black) plasmids. (d) Detection of GFP expression by sodium dodecyl sulfate (SDS)-PAGE gel. The *in vitro* transcription and translation samples were separated on SDS-PAGE and stained with Coomassie brilliant blue for the GFP expression confirmation. The arrowhead indicates the GFP in the respective samples. The purified GFP was used as a control and to determine the exact sized band expected.

(50 ng DNA and 150 ng SWCNT) complex was used as a template in a PCR to amplify a fragment of DNA from the plasmid condensed on the PEI_{30}-$SWCNT^{+61mV}$. The results showed no amplification of the respective DNA fragment compared to proper amplification from the control plasmid (Figure S19b). This confirms that the DNA bound to PEI-SWCNTs is not available to the DNA polymerase for PCR amplification.

Because the binding of DNA to the PEI_{30}-$SWCNT^{+61mV}$ is charge-dependent, an increased change in pH or high salt concentration could favor surface charge neutralization and the subsequent release of DNA. To that end, PCR was performed in Tris buffer (pH = 9). Similar to previous results, PCR did not amplify the respective DNA fragment compared to the proper amplification from the control vectors with two different primer sets (Figure S19c). Similarly, we found that increasing the salt concentration up to 1 M NaCl, an order of magnitude higher than the physiological ionic strength, did not release the condensed DNA from the PEI_{30}-$SWCNT^{+61mV}$. Next, the DNA-PEI_{30}-$SWCNT^{+61mV}$ conjugation was carried out in the presence of different salts. Gel electrophoresis results confirmed no release of the DNA from the DNA- PEI_{30}-$SWCNT^{+61mV}$ complex (Figure S20a). Similarly, the sequential addition of salts did not release the DNA from the PEI_{30}-$SWCNT^{+61mV}$-DNA complex (Figure S20b). These results confirm that DNA is strongly held to the surface of the PEI_{30}-$SWCNT^{+61mV}$, irrespective of its binding mode, and suggest that the complex undergoes no physical changes under conditions of high pH or

high salt concentration, including physiological pH and ionic strength.

Investigation of the Effect of Plasmid Size and the Gene-to-Plasmid Ratio on the Expression Level of the GFP. We showed that the binding mode of plasmid DNA to PEI-SWCNTs is a key factor that governs the successful expression of GFP. However, this does not explain the failure of DNA expression of large functional DNA units on the multiple plasmids used in our experiments. Our AFM results (Figures 5 and S14) suggest that the GFP expression is likely to originate from the uncondensed parts of partially condensed DNA (free and thus available to the cellular transcription machinery (Figures 5h and S14)) but not from the extended or condensed parts (strongly bound to the PEI-SWCNTs and thus unavailable to the cellular transcription machinery (DNA-1 and DNA-2 in Figure 5e)). Protein expression requires the availability of the promoter sequence for RNA polymerase binding and the open reading frame (ORF) sequence for RNA transcript synthesis and the termination signal sequence followed by translation and polypeptide formation. Thus, considering the limited size of the uncondensed parts of partially condensed DNA and the irreversible binding of DNA to PEI-SWCNTs (see above), we hypothesized that a gene with a short sequence would be more likely to be fully accessible in the uncondensed parts of the DNA and thus more likely to be available to the cellular transcription machinery. By contrast, a gene with a long sequence is more likely to be present in both the condensed and uncondensed conformations and, hence, would not be fully available to the transcription machinery. These differences in the condensed

conformations of the plasmid and thus the probability of accessibility of the genes could lead to facilitated transcription of small genes and hindered transcription of long genes (ORFs).

To explore this hypothesis and to confirm the availability of the DNA sequence for polymerase processing, a GFP expression cassette (1.3 kb) was cloned into two plasmids with different sizes (3.2 and 12 kb, Figure 6a). A short 1.3 kb ORF gene sequence is more likely to be present fully in the uncondensed parts of the DNA of a 12 kb plasmid and thus available to the cellular transcription machinery for expression. In contrast, the same short ORF on a 3.2 kb plasmid is more likely to strongly condense on the PEI_{30}-$SWCNT^{+61mV}$ and, therefore, we hypothesize that the ORF sequence is relatively less available to the transcription machinery. The constructed plasmid DNAs were conjugated at a 1:3 ratio with the PEI_{30}-SWCNTs and were subjected to a cell-free protein expression system. A low GFP expression signal was detected from GFP cassettes cloned onto the 12 kb plasmid under UV light, but only a minimal GFP signal was observed from the GFP cassette cloned onto the small plasmid (Figure 6b−d). The *in vitro* transcription results suggest the availability of the GFP cassette when cloned into the 12 kb plasmid and conjugated onto the PEI_{30}-$SWCNT^{+61mV}$ but poor or no availability for expression from the small (3.2 kb) plasmid harboring the GFP cassette conjugated to the PEI_{30}-$SWCNT^{+61mV}$. The unbound plasmid DNA was used as a positive expression control. This data demonstrated that the relative size of the gene with respect to the plasmid size determines the expression efficiency *in vitro* in the plasmid DNA bound to PEI_{30}-$SWCNT^{+61mV}$ composites and its putative accessibility once inside the plant cell.

These results clearly demonstrate that by increasing the DNA size, the probability that the expression cassette remains fully exposed to the expression machinery increases accordingly. This allows proper expression of the genetic cassette (Figure 6b). The size limit of the gene suitable for expression using the PEI_{30}-$SWCNT^{+61mV}$ module and the optimal gene-to-plasmid ratio remains to be explored.

CONCLUSIONS

We show that the efficiency of *in planta* DNA expression from PEI-SWCNT carriers is largely affected by several biological and physical factors. The cell wall remains the first barrier where the limited size of cell wall pores impedes the passage of large-sized PEI-SWCNT-DNA composites (*i.e.*, $PEI_{0.1}$-SWCNT-DNA, Figure 5i) where DNA is more exposed to the transcription machinery than to smaller SWCNT-DNA composites (*i.e.*, PEI_{30}-SWCNT-DNA). Thus, a sufficiently high surface potential of the PEI-SWCNT is required to condense the DNA efficiently and decrease the size of the composite. In addition, increasing the DNA concentration often leads to precipitation of the composites due to opposite charge attraction. Furthermore, our results indicate that the distribution of the positively charged PEI on the surface of the SWCNT induces DNA to bind in different modes and that only composites with partially condensed DNA are expressed inside the cells. This partial condensation limits the size of the gene that can be expressed because the condensed DNA is not released from the PEI_{30}-SWCNT and, thus, part of the DNA sequences are unavailable to the cellular transcription machinery. Combined, this study provides an important implication that the efficient condensation of the DNA, which is a prerequisite for cell wall trafficking, and good accessibility of the transcription machinery to the condensed DNA in the cell nucleus as a

prerequisite for an efficient expression of the delivered gene, are hard to achieve simultaneously using the module of charge-based DNA loading onto PEI-coated SWCNTs. This trade-off may pose a challenge to utilize the PEI-SWCNT-mediated gene delivery for efficient genome engineering applications in plants, which require large multi-unit plasmid constructs. The binding modes of DNA could be controlled if one can control the spatial pattern of the PEI coating layer on the SWCNT. However, the spatial distribution of COOH groups on the SWCNTs that are chemically conjugated to PEI is hard to control during the synthesis of COOH-SWCNTs. Thus, our results strongly suggest that the development of a method enabling not only tight condensation of DNA on the carrier but also good access through the cell wall and good access of the transcription machinery to the delivered DNA would be the key for the future development of the nanomaterial-based gene delivery to plants. We are currently developing advanced fluorescence imaging techniques (*e.g.*, shortwave infrared imaging, multiphoton imaging, and time-gated imaging) to directly visualize spatiotemporal behavior of the SWCNT nanocarriers and DNA bound to the nanocarriers inside intact plants at the single-molecule (nanocarrier) level. Studies along this direction would fully unravel complicated molecular mechanisms that control the delivery and expression of DNA in plants.

MATERIALS AND METHODS

PEI-SWCNT Preparation. PEI-SWCNTs were prepared following the procedures described by Demirer et al.[30] All chemicals and equipment of the exact catalogue numbers mentioned in the Demirer et al. protocol were used in the preparation of PEI-SWCNTs. Briefly, 30 mg of carboxylated SWCNTs (COOH-SWCNTs) were added to 30 mL nuclease-free water and bath sonicated for 10 min, and then tip sonicated (6 mm probe 10% amplitude) for 30 min on ice. COOH-SWCNTs were centrifuged for 1 h at 18 000 rpm, and the supernatant was collected. COOH-SWCNTs (2 mg) were reacted with 10 mg of 1-ethyl-3-[3-dimethylaminopropyl] carbodiimide hydrochloride (EDC) and 10 mg of *N*-hydroxysuccinimide (NHS) in 100 mM MES buffer (pH 4.5−5). After bath sonication for 10 min, the reaction was continued for 1 h on an orbital shaker at 180 rpm. Excess NHS and EDC were removed, and MES buffer was replaced with 0.1 PBS, pH 7.4, by washing the samples on a 100 kDa filter three times. The EDC- and NHS-reacted COOH-SWCNTs were reacted with 0.1, 20, 30, 40, and 60 mg of PEI (25 000 MW, branched). The reaction was continued for 12 h on an orbital shaker at 180 rpm. The PEI-SWCNT samples were washed with nuclease-free water seven times on a 100 kDa filter. The PEI-SWCNTs were bath sonicated for 15 min and then probe sonicated for 15 min on ice. The PEI-SWCNTs were then centrifuged for 1 h at 16 000 rpm, and the supernatant was collected. The ζ potential measurement was used to judge the quality of the synthesis (see Text S5). We note that we were able to obtain reproducible results using the PEI_{30}-SWCNT but not using the PEI_{20}-SWCNT. The latter consistently showed a ζ potential value of <+60 mV at normal incubation conditions and inconsistently showed a ζ potential value of ∼+60 mV by increasing the incubation time to 18 h. Thus, we presented and discussed the results of the working PEI-SWCNT composite (PEI_{30}-SWCNT). All chemicals and equipment used in this study are listed in the Supporting Information.

Plasmids and Constructs. To make a 10.6 kb vector expressing mGFP, the binary vector pMDC43 was modified by removing the Gateway cassette of *ccdB* and *CMR* genes after the mGFP open reading frame (ORF). The same GFP ORF with its 35SCaMV promoter and Nos terminator was also cloned into the pJet2.1 vector to make a 4.8 kb fragment. pJL-TRBO-G was used to express the GFP from the TMV plasmid. For the BFP, the GFP in pJL-TRBO-G was replaced with the BFP. For the VIGS assay, a short sequence of the *N. benthamiana PDS* gene was cloned into the RNA2 genome of TRV and used with RNA1 for *PDS* gene silencing. For systemic GFP assays, PVX-GFP was used.

For viral symptomatic analysis, a binary vector containing TYLCV2.3 was used. For *in vitro* transcription and translation assays, the pQ70-deGFP vector (3.2 kb) and a plasmid of 12.3 kb were made by cloning the same GFP expression cassette with its Q70 promoter and terminator. Maps of the plasmids used are provided in the Supporting Information.

DNA Binding Assays. PEI-SWCNTs (300 ng) were added to either 300, 150, or 100 ng of plasmid DNA in nuclease-free water and incubated for 30 min. To confirm the effect of salts on DNA release from PEI-SWCNTs, $MgCl_2$, KCl, and NaCl (5 and 10 mM) were added directly or sequentially. The DNA-PEI-SWCNT complex was separated on a 1% agarose gel.

Infiltrations. Three-week-old soil-grown *N. benthamiana* plants were used in all experiments. The PEI-SWCNTs prepared were used directly or maximum in the first week of synthesis. PEI-SWCNTs were always probe-tip sonicated prior to use. PEI-SWCNTs were added to DNA at the ratios of 3:1, 2:1, and 1:1 in infiltration buffer ($MgCl_2$ and MES, pH 6). The DNA-PEI-SWCNT complexes were infiltrated into the lower epidermis of fully expanded leaves. In all experiments, the ratio of the DNA/PEI-SWCNT was 1:3, which was the optimal ratio that generated a stable solution and better expression, except otherwise indicated in the respective figures' legends.

GFP Expression Analysis Using a Confocal Microscope. The pDNA−PEI-SWCNT complex (100−200 μL solution) was infiltrated with a 1 mL needless syringe to the abaxial surface of fully expanded true leaves of 3 weeks old *N. benthamiana* plants. Plants infiltrated with pDNA-PEI-SWCNTs were placed in the plant growth chamber to allow plasmid internalization and proper expression for 3−7 days. The infiltrated leaves were analyzed for GFP expression after 3 days (for normal plasmids) and 7 days (for the TURBO-G-based GFP expression system) with a confocal microscope. Confocal microscopy was performed at 20× lenses using a Zeiss LSM 710 inverted confocal microscope.

Western Blot. The total proteins were extracted in buffer (100 mM Tris−HCl, pH 7.5, 150 mM NaCl, 0.5% NP-40, 1 mM ethylenediaminetetraacetic acid (EDTA), 3 mM dithiothreitol (DTT), and protease inhibitors) and separated on a 12% polyacrylamide gel. Proteins were blotted onto a nitrocellulose membrane. The immunoblot was incubated with the primary antibody (anti-GFP antibody, Abcam) at 1:5000 at room temperature for 1 h and anti-IgG at 1:5000 for 1 h. After treatment with ECL (SuperSignal West Pico Plus Thermo Fisher Scientific), the GFP signal was detected with a ImageQuant LAS4000 (GE Healthcare).

DNA Accessibility Assay. PCR was performed to confirm the accessibility of the PEI-SWCNT-loaded DNA (3:1). The DNA-PEI-SWCNT complex was used as a template in the PCR using the NEB high fidelity Phusion protocol. To confirm the pH effect on DNA accessibility, PCR was carried out at pH 9. The plasmid was used as a control.

***In Vitro* Transcription and Translation Assay.** A cell-free protein expression kit (Arbor Biosciences) was used for *in vitro* transcription and translation assays. The plasmid pQ70-deGFP vector (3.2 kb) and the 12.3 kb plasmid were loaded onto PEI-SWCNTs and then used as templates as per the recommendation of the protocol. Reaction tubes were imaged under UV in the dark room.

PEI-SWCNT-Based Plasmid Transformation and Viral Infection. To transform plasmid and virus infection clones into plants, plasmids and vectors containing the infectious clones of TMV, TRV, PVX, and TYLCV were loaded onto PEI-SWCNTs in ratios of 1:1 and 1:3 and infiltrated into the lower epidermis of *N. benthamiana* leaves. All transformation experiments were repeated (three plants per set) three times, and the results were consistent among the replicates. Maps of all of the plasmids are provided in the Supporting Information.

***Agrobacterium*-Based Plasmid Transformation and Viral Infection.** *Agrobacterium* was used as a control for the delivery of plasmids and viral genomes on T-DNA plasmids into the plant cells *via* infiltration. Binary plasmids were transformed into *Agrobacterium* by electroporation, and the cells were selected on the respected antibiotic plates. A single colony of the transformed *Agrobacterium* was grown in LB media. The cells were collected by centrifugation, resuspended in the infiltration buffer, and infiltrated to *N. benthamiana* leaves.

Rolling Circle Amplification Assay. Total DNA from the young systemic leaves was isolated seven days after infiltration. The isolated DNA was subjected to RCA using a Templiphi 100 Amplification kit (catalogue number 25640010, GE HealthCare) and protocol. The amplicons were linearized with *Nco*I and separated on 1% agarose gel.

One-Step RT-qPCR. Total RNA from the infiltrated leaves was isolated 3 days after infiltration using DirectZol (RNA miniprep kit, ZymoResearch, cat. no. R2072). The isolated RNA was treated with DNaseI and subjected to RT-qPCR, using an iTaq universal SYBR Green One-Step kit (catalogue number 1725150, BioRad) as per the standard protocol. The PP2A gene was used as a plant internal expression reference. The primer sequence used for the GFP and PP2A is provided in the Supporting Information.

Quasielastic Light Scattering (QELS) and ζ Potential Measurements. Solutions of SWCNTs, PEI-SWCNTs, and DNA-PEI-SWCNTs were diluted to a final concentration of 7 μg mL^{-1}. QELS and ζ potential data were acquired using a Malvern Zetasizer Nano-ZS (Malvern, Worcestershire, U.K.). The system was equipped with a HeNe laser (633 nm) and was capable of measuring the size of particles of 0.3 nm to 10 μm. Data were analyzed using Zetasizer (Malvern) and OriginPro (Originlabs) software. The polydispersity index of the original QELS distributions was calculated using Zetasizer software. The ζ potentials of the three independent PEI$_{30}$-SWCNT samples are +61.3, +63.6, and 67.4 mV, whereas the values of the PEI$_{20}$-SWCNT samples are +52.4, +53.5, and 56.1 mV. We used the lowest ζ potential to denote each sample, namely, PEI$_{30}$-SWCNT^{+61mV} and PEI$_{20}$-SWCNT^{+52mV}, respectively.

Atomic Force Microscopy (AFM) Imaging. To conduct dry-phase AFM, a few microliters of SWCNT, PEI-SWCNT, or DNA-PEI-SWCNT solutions were deposited on a freshly cleaved mica surface and vacuum dried. To conduct solution-phase AFM, 10 μL of a DNA-PEI-SWCNT solution in 10 mM TE buffer was deposited on a freshly cleaved mica surface and incubated at room temperature for 5 min, and then washed with 200 μL Milli-Q water. AFM imaging was performed in 1 mM Tris buffer (pH = 7.5) with an Agilent 5500 Scanning Probe Microscope (Agilent Technologies, CA) using silicon nitride tips (AC40, Bruker) in AAC mode (tapping mode) with a scan rate of 1 Hz and an amplitude set point of 0.9−1.2 V. Images were collected at 1 μm × 1 μm or 0.5 μm × 0.5 μm scans. To obtain the liquid-phase AFM images shown in Figure S10, the TRBO-DNA-PEI$_{30}$-SWCNT^{+61mV} complex was suspended in the infiltration buffer. One milliliter of the suspension was deposited on the surface of freshly cleaved mica fixed inside a small plastic dish (Corning, NY), incubated for 1 h, and then imaged using a SCANASYST-FLUID+ cantilever (Bruker). We obtained approximately 100 images of each preparation and identified 70 tubes in each sample, whereas images showing excessive artifacts were discarded. The binding modes of DNA on the PEI-SWCNT (*i.e.*, extended, condensed, and partially condensed modes) were systematically analyzed. The extended mode of binding was identified by following the method described in ref 26, whereas the condensed DNA was distinguished from the artifacts by the method described in Text S1. The partially condensed mode of binding of DNA was identified *via* the presence of lobes of DNA extruded from the condensed DNA (see Figures 5h and S16).

Scanning Kelvin Probe Microscopy Imaging (SKPM). PEI-SWCNTs at a concentration of 1 μg mL^{-1} were deposited on a Cr/Au (10/200 nm) Si substrate to provide a conductive uniform substrate for the Kelvin probe measurements. The Kelvin probe was performed by means of an Oxford Instruments Asylum research MFP-3D equipped with Asylum cantilever Ti/Ir tips (nominal resonant frequency = 75 kHz, spring constant = 2 N m^{-1}, and a nominal tip curvature radius of 30 nm) in a dual-pass mode (NAP mode) at a second pass elevation of 50 nm. To compute the sample work function, the tip was carefully calibrated on a freshly cleaved Bernal-stacked HOPG sample (ZYA, NT-MDT) with a nominal work function of 4.6 eV and a uniformity of 1.8 mV$_{rms}$, taken as measurement accuracy, using the same parameters. To avoid water condensation at the surface, all measurements and

calibrations were performed in a reduced humidity environment of RH <3%.

Fluorescence Spectroscopy. Fluorescence measurement of the GFP was performed using spectrofluorometer Fluoromax-4 (Horiba Scientific, Japan). Fluorescence spectra of the GFP were measured upon excitation at 488 nm. The integrated fluorescence intensity (area under the peak) was calculated using OriginPro (Originlabs) software.

ASSOCIATED CONTENT

Supporting Information

The Supporting Information is available free of charge at https://pubs.acs.org/doi/10.1021/acsanm.1c03482.

Detection of binding modes of DNA (Text S1); detection level sensitivity of western blotting (Text S2); employment of dynamic light scattering to measure the experimental hydrodynamic diameter of carbon nanotubes (Text S3); physical characteristics of PEI and chitosan (Text S4); batch-to-batch variation of the synthesized PEI-SWCNT (Text S5); relationship between the charge density along the PEI-SWCNTs and the binding mode of the plasmid DNA (Text S6); supporting figures and tables; supporting reagents and equipment; AFM topographic views of PEI_{20}-$SWCNT^{+52mV}$ (Appendix S1); AFM topographic views of PEI_{20}-$SWCNT^{+61mV}$ (Appendix S2); maps of the plasmid used in this study (PDF)

AUTHOR INFORMATION

Corresponding Authors

Satoshi Habuchi — *Biological and Environmental Sciences and Engineering Division, King Abdullah University of Science and Technology (KAUST), Thuwal 23955-6900, Saudi Arabia;* orcid.org/0000-0002-6663-2807; Email: Satoshi.Habuchi@kaust.edu.sa

Magdy Mahfouz — *Laboratory for Genome Engineering and Synthetic Biology, Division of Biological Sciences, 4700 King Abdullah University of Science and Technology, Thuwal 23955-6900, Saudi Arabia;* orcid.org/0000-0002-0616-6365; Email: magdy.mahfouz@kaust.edu.sa

Authors

Zahir Ali — *Laboratory for Genome Engineering and Synthetic Biology, Division of Biological Sciences, 4700 King Abdullah University of Science and Technology, Thuwal 23955-6900, Saudi Arabia*

Maged F. Serag — *Biological and Environmental Sciences and Engineering Division, King Abdullah University of Science and Technology (KAUST), Thuwal 23955-6900, Saudi Arabia*

Gozde S. Demirer — *Department of Chemical Engineering, California Institute of Technology, Pasadena, California 91125, United States*

Bruno Torre — *SMILEs Lab, Physical Science and Engineering (PSE), King Abdullah University of Science and Technology, Thuwal 23955-6900, Saudi Arabia; Department of Applied Science and Technology (DISAT), Politecnico di Torino, 10129 Torino, Italy*

Enzo di Fabrizio — *SMILEs Lab, Physical Science and Engineering (PSE), King Abdullah University of Science and Technology, Thuwal 23955-6900, Saudi Arabia; Department of Applied Science and Technology (DISAT), Politecnico di Torino, 10129 Torino, Italy*

Markita P. Landry — *Department of Chemical and Biomolecular Engineering, University of California, Berkeley, California 94720-1460, United States;* orcid.org/0000-0002-5832-8522

Complete contact information is available at:
https://pubs.acs.org/10.1021/acsanm.1c03482

Author Contributions

◆Z.A. and M.F.S. contributed equally to this work. M.M.M., S.H., and M.P.L. conceived research. Z.A. and M.F.S. designed the research. Z.A., M.F.S., G.S.D., and B.T. performed the research. Z.A., M.F.S., M.M.M., and S.H. wrote the paper with input from M.P.L., G.S.D., M.F.S., B.T., and E.d.F.

Notes

The authors declare no competing financial interest.

ACKNOWLEDGMENTS

REFERENCES

(1) Zaidi, S. S.; Vanderschuren, H.; Qaim, M.; Mahfouz, M. M.; Kohli, A.; Mansoor, S.; Tester, M. New Plant Breeding Technologies for Food Security. *Science* **2019**, *363*, 1390−1391.

(2) Jenkins, T.; Bovi, A.; Edwards, R. Plants: Biofactories for a Sustainable Future? *Philos. Trans. R. Soc., A* **2011**, *369*, 1826−1839.

(3) Schmitz, D.; Ali, Z.; Wang, C.; Aljedaani, F.; Hooykaas, P.; Mahfouz, M.; Pater, S. CRISPR/Cas9 Mutagenesis by Translocation of Cas9 Protein Into Plant Cells via the Agrobacterium Type IV Secretion System. *Front. Genome Ed.* **2020**, *2*, No. 6.

(4) Ali, Z.; Abul-faraj, A.; Li, L.; Ghosh, N.; Piatek, M.; Mahjoub, A.; Aouida, M.; Piatek, A.; Baltes, N. J.; Voytas, D. F.; Dinesh-Kumar, S.; Mahfouz, M. M. Efficient Virus-Mediated Genome Editing in Plants Using the CRISPR/Cas9 System. *Mol. Plant* **2015**, *8*, 1288−1291.

(5) Carpita, N.; Sabularse, D.; Montezinos, D.; Delmer, D. P. Determination of the Pore Size of Cell Walls of Living Plant Cells. *Science* **1979**, *205*, 1144−1147.

(6) Baron-Epel, O.; Gharyal, P. K.; Schindler, M. Pectins as Mediators of Wall Porosity in Soybean Cells. *Planta* **1988**, *175*, 389−395.

(7) Gelvin, S. B. The Introduction and Expression of Transgenes in Plants. *Curr. Opin. Biotechnol.* **1998**, *9*, 227−232.

(8) Chung, S. M.; Vaidya, M.; Tzfira, T. Agrobacterium is Not Alone: Gene Transfer to Plants by Viruses and Other Bacteria. *Trends Plant Sci.* **2006**, *11*, 1−4.

(9) Kaeppler, H. F.; Somers, D. A.; Rines, H. W.; Cockburn, A. F. Silicon Carbide Fiber-Mediated Stable Transformation of Plant Cells. *Theor. Appl. Genet.* **1992**, *84−84*, 560−566.

(10) Gao, C.; Nielsen, K. K. Comparison Between Agrobacterium-Mediated and Direct Gene Transfer Using the Gene Gun. *Biolistic DNA Delivery*; Methods in Molecular Biology; Humana Press, 2013; Vol. 6, pp 3−16.

(11) Chichiriccò, G.; Poma, A. Penetration and Toxicity of Nanomaterials in Higher Plants. *Nanomaterials* **2015**, *5*, 851−873.

(12) Kam, N. W. S.; O'Connell, M.; Wisdom, J. A.; Dai, H. Carbon nanotubes as multifunctional biological transporters and near-infrared agents for selective cancer cell destruction. *Proc. Natl. Acad. Sci. U.S.A.* **2005**, *102*, 11600−11605.

(13) Serag, M. F.; Kaji, N.; Tokeshi, M.; Baba, Y. Introducing Carbon Nanotubes into Living Walled Plant Cells Through Cellulase-Induced Nanoholes. *RSC Adv.* **2012**, *2*, 398−400.

(14) Bianco, A.; Kostarelos, K.; Prato, M. Making carbon nanotubes biocompatible and biodegradable. *Chem. Commun.* **2011**, *47*, 10182−10188.

(15) Serag, M. F.; Kaji, N.; Habuchi, S.; Bianco, A.; Baba, Y. Nanobiotechnology Meets Plant Cell Biology: Carbon Nanotubes as Organelle Targeting Nanocarriers. *RSC Adv.* **2013**, *3*, 4856−4862.

(16) Serag, M. F.; Braeckmans, K.; Habuchi, S.; Kaji, N.; Bianco, A.; Baba, Y. Spatiotemporal Visualization of Subcellular Dynamics of Carbon Nanotubes. *Nano Lett.* **2012**, *12*, 6145−6151.

(17) Lin, Y.; Taylor, S.; Li, H.; Shiral Fernando, K. A.; Qu, L.; Wang, W.; Gu, L.; Zhou, B.; Sun, Y. Advances toward bioapplications of carbon nanotubes. *J. Mater. Chem.* **2004**, 527−541.

(18) Mitter, N.; Worrall, E. A.; Robinson, K. E.; Li, P.; Jain, R. G.; Taochy, C.; Fletcher, S. J.; Carroll, B. J.; Lu, G. Q.; Xu, Z. P. Clay Nanosheets for Topical Delivery of RNAi for Sustained Protection Against Plant Viruses. *Nat. Plants* **2017**, *3*, No. 16207.

(19) Bao, W.; Wang, J.; Wang, Q.; O'Hare, D.; Wan, Y. Layered Double Hydroxide Nanotransporter for Molecule Delivery to Intact Plant Cells. *Sci. Rep.* **2016**, *6*, No. 26738.

(20) Zhang, H.; Demirer, G. S.; Zhang, H.; Ye, T.; Goh, N. S.; Aditham, A. J.; Cunningham, F. J.; Fan, C.; Landry, M. P. DNA Nanostructures Coordinate Gene Silencing in Mature Plants. *Proc. Natl. Acad. Sci. U.S.A.* **2019**, *116*, 7543−7548.

(21) Demirer, G. S.; Zhang, H.; Goh, N. S.; Pinals, R. L.; Chang, R.; Landry, M. P. Carbon Nanocarriers Deliver siRNA to Intact Plant Cells for Efficient Gene Knockdown. *Sci. Adv.* **2020**, *6*, No. eaaz0495.

(22) Torney, F.; Trewyn, B. G.; Lin, V. S. Y.; Wang, K. Mesoporous Silica Nanoparticles Deliver DNA and Chemicals into Plants. *Nat. Nanotechnol.* **2007**, *2*, 295−300.

(23) Wang, B.; Huang, J.; Zhang, M.; Wang, Y.; Wang, H.; Ma, Y.; Zhao, X.; Wang, X.; Liu, C.; Huang, H.; Liu, Y.; Lu, F.; Yu, H.; Shao, M.; Kang, Z. Carbon Dots Enable Efficient Delivery of Functional DNA in Plants. *ACS Appl. Bio Mater.* **2020**, *3*, 8857−8864.

(24) Schwartz, S. H.; Hendrix, B.; Hoffer, P.; Sanders, R. A.; Zheng, W. Carbon Dots for Efficient Small Interfering RNA Delivery and Gene Silencing in Plants. *Plant Physiol.* **2020**, *184*, 647−657.

(25) Demirer, G. S.; Zhang, H.; Matos, J. L.; Goh, N. S.; Cunningham, F. J.; Sung, Y.; Chang, R.; Aditham, A. J.; Chio, L.; Cho, M. J.; Staskawicz, B.; Landry, M. P. High Aspect Ratio Nanomaterials Enable Delivery of Functional Genetic Material Without DNA Integration in Mature Plants. *Nat. Nanotechnol.* **2019**, *14*, 456−464.

(26) Kwak, S. Y.; Lew, T. T. S.; Sweeney, C. J.; Koman, V. B.; Wong, M. H.; Bohmert-Tatarev, K.; Snell, K. D.; Seo, J. S.; Chua, N. H.; Strano, M. S. Chloroplast-Selective Gene Delivery and Expression in Planta Using Chitosan-Complexed Single-Walled Carbon Nanotube Carriers. *Nat. Nanotechnol.* **2019**, *14*, 447−455.

(27) Lew, T. T. S.; Park, M.; Wang, Y.; Gordiichuk, P.; Yeap, W.-C.; Mohd Rais, S. K.; Kulaveerasingam, H.; Strano, M. S. Nanocarriers for Transgene Expression in Pollen as a Plant Biotechnology Tool. *ACS Mater. Lett.* **2020**, *2*, 1057−1066.

(28) Behnam, B.; Shier, W. T.; Nia, A. H.; Abnous, K.; Ramezani, M. Non-Novalent Functionalization of Single-Walled Carbon Nanotubes with Modified Polyethyleneimines for Efficient Gene Delivery. *Int. J. Pharm.* **2013**, *454*, 204−215.

(29) Golestanipour, A.; Nikkhah, M.; Aalami, A.; Hosseinkhani, S. Gene Delivery to Tobacco Root Cells with Single-Walled Carbon Nanotubes and Cell-Penetrating Fusogenic Peptides. *Mol. Biotechnol.* **2018**, *60*, 863−878.

(30) Demirer, G. S.; Zhang, H.; Goh, N. S.; Gonzalez-Grandio, E.; Landry, M. P. Carbon Nanotube-Mediated DNA Delivery Without Transgene Integration in Intact Plants. *Nat. Protoc.* **2019**, *14*, 2954−2971.

(31) Wu, Y.; Phillips, J. A.; Liu, H.; Yang, R.; Tan, W. Carbon Nanotubes Protect DNA Strands During Cellular Delivery. *ACS Nano* **2008**, *2*, 2023−2028.

(32) Cunningham, F. J.; Goh, N. S.; Demirer, G. S.; Matos, J. L.; Landry, M. P. Nanoparticle-Mediated Delivery towards Advancing Plant Genetic Engineering. *Trends Biotechnol.* **2018**, *36*, 882−897.

(33) Giraldo, J. P.; Wu, H.; Newkirk, G. M.; Kruss, S. Nano-biotechnology Approaches for Engineering Smart Plant Sensors. *Nat. Nanotechnol.* **2019**, *14*, 541−553.

(34) Ali, Z.; Shami, A.; Sedeek, K.; Kamel, R.; Alhabsi, A.; Tehseen, M.; Hassan, N.; Butt, H.; Kababji, A.; Hamdan, S. M.; Mahfouz, M. M. Fusion of the Cas9 Endonuclease and the VirD2 Relaxase Facilitates Homology-Directed Repair for Precise Genome Engineering in Rice. *Commun. Biol.* **2020**, *3*, No. 44.

(35) Lindbo, J. A. TRBO: a High-Efficiency Tobacco Mosaic Virus RNA-Based Overexpression Vector. *Plant Physiol.* **2007**, *145*, 1232−1240.

(36) Whitfield, A. E.; Falk, B. W.; Rotenberg, D. Insect vector-Mediated Transmission of Plant Viruses. *Virology* **2015**, *479-480*, 278−289.

(37) Dietzgen, R. G.; Mann, K. S.; Johnson, K. N. Plant Virus-Insect Vector Interactions: Current and Potential Future Research Directions. *Viruses* **2016**, *8*, No. 303.

(38) Hull, R. Replication of Plant Viruses. *Plant Virology*, 5th ed.; Elsevier: Amsterdam, 2014; Vol. 8, pp 341−421.

(39) Moriones, E.; Navas-Castillo, J. Tomato Yellow Leaf Curl Virus, an Emerging Virus Complex Causing Epidemics Worldwide. *Virus Res.* **2000**, *71*, 123−134.

(40) Hayward, A.; Padmanabhan, M.; Dinesh-Kumar, S. P. Virus-Induced Gene Silencing in *Nicotiana benthamiana* and Other Plant Species. *Plant Reverse Genetics*; Methods in Molecular Biology; Humana Press, 2011; Vol. *678*, pp 55−63.

(41) Cruz, S. S.; Chapman, S.; Roberts, A. G.; Roberts, I. M.; Prior, D. A.; Oparka, K. J. Assembly and Movement of a Plant Virus Carrying a Green Fluorescent Protein Overcoat. *Proc. Natl. Acad. Sci. U.S.A.* **1996**, *93*, 6286−6290.

(42) Gong, X.; Sharma, A. K.; Strano, M. S.; Mukhopadhyay, D. Selective Assembly of DNA-Conjugated Single-Walled Carbon Nanotubes from the Vascular Secretome. *ACS Nano* **2014**, *8*, 9126−9136.

(43) Manning, G. S. Counterion Condensation Theory of Attraction Between Like Charges in the Absence of Multivalent Counterions. *Eur. Phys. J. E: Soft Matter Biol. Phys.* **2011**, *34*, No. 132.

(44) Sergei, V.; Kalinin, A. G. *Scanning Probe Microscopy: Electrical and Electromechanical Phenomena at the Nanoscale*; Springer Science & Business Media, 2007; p 980.

(45) Lanza, M. *Conductive Atomic Force Microscopy: Applications in Nanomaterials*; John Wiley & Sons, 2017; p 384.